Published in final edited form as:

Nat Rev Mater. 2018 April ; 3(4): . doi:10.1038/natrevmats.2018.16.

Nanofibrils in nature and materials engineering

Shengjie Ling[1,2,3], **David L. Kaplan**[3,*], **Markus J. Buehler**[2,4,5,*]

[1]School of Physical Science and Technology, ShanghaiTech University, Shanghai, China

[2]Department of Civil and Environmental Engineering, Massachusetts Institute of Technology, Cambridge, MA, USA

[3]Department of Biomedical Engineering, Tufts University, Medford, MA, USA

[4]Center for Materials Science and Engineering, Massachusetts Institute of Technology, Cambridge, MA, USA

[5]Center for Computational Engineering, Massachusetts Institute of Technology, Cambridge, MA, USA

Abstract

Nanofibrillar materials, such as cellulose, chitin and silk, are highly ordered architectures, formed through the self-assembly of repetitive building blocks into higher-order structures, which are stabilized by non-covalent interactions. This hierarchical building principle endows many biological materials with remarkable mechanical strength, anisotropy, flexibility and optical properties, such as structural colour. These features make nanofibrillar biopolymers interesting candidates for the development of strong, sustainable and biocompatible materials for environmental, energy, optical and biomedical applications. However, recreating their architecture is challenging from an engineering perspective. Rational design approaches, applying a combination of theoretical and experimental protocols, have enabled the design of biopolymer-based materials through mimicking nature's multiscale assembly approach. In this Review, we summarize hierarchical design strategies of cellulose, silk and chitin, focusing on nanoconfinement, fibrillar orientation and alignment in 2D and 3D structures. These multiscale architectures are discussed in the context of mechanical and optical properties, and different fabrication strategies for the manufacturing of biopolymer nanofibril-based materials are investigated. We highlight the contribution of rational material design strategies to the development of mechanically anisotropic and responsive materials and examine the future of the material-by-design paradigm.

Biopolymer nanofibrils constitute the basic architectural element of many biological materials that fulfil structural functions[1–3]. Cellulose nanofibrils in plants and bacteria, chitin nanofibrils in animals and silk fibroin nanofibrils from spiders and silkworms share

* David.Kaplan@Tufts.edu; mbuehler@mit.edu.

Author contributions

All authors contributed equally to the preparation of this manuscript.

Competing interests

The authors declare no competing interests.

common hierarchical structural motifs, designed to provide mechanical strength and a structural scaffold (FIG. 1). Biopolymer nanofibrils consist of repetitive core sequences, such as hydrophilic and hydrophobic segments of amino acids in silk, β-(1,4)-linked d-glucose units in cellulose and a long-chain polymer of (1,4)-β-*N*-acetylglucosamine, a derivative of glucose, in chitin. The polymer chains assemble into semicrystalline structures with alternating amorphous and nanocrystalline regions, which are stabilized by hydrogen bonds and van der Waals forces[4–6]. The size of the respective nanocrystal unit is typically confined to several nanometres (approximately 2–5 nm for cellulose and chitin nanocrystals and silk β-sheets). Nanoconfinement to this length scale allows for the most efficient use of hydrogen bonds in order to maximize stiffness, strength and toughness[7–9]. The amorphous and nanocrystal components are organized as nanofibrils, which are bundled into fibrils with diameters of ~20–100 nm, up to the micrometre scale, and a fibrillar orientation along the longitudinal fibre axis. In wood, fruits and arthropod exoskeletons, cellulose and chitin nanofibrils are further stacked into higher-order 2D laminar (for example, in wood cell walls and in the exoskeleton of lobsters) or 3D helicoidal structures, also called twisted plywood or Bouligand structures (for example, in fruit peel and arthropod exoskeletons)[10] (FIG. 1). In higher-order plants, the 2D laminar stacks are formed of cellulose fibrils that are additionally embedded in a matrix of amorphous hemicellulose and lignin to form the mature layered cell wall, whereas in the exoskeleton of arthropods, chitin nanofibrils are confined by a sheath of proteins and assembled into elongated fibrils that are embedded in a mineral–protein matrix. The chitin–protein fibrils align as planar layers along their normal direction with helicoidal stacking, that is, adjacent fibre layers are rotated by a constant angle, and the arrangement completes a full 180° rotation.

This multiscale construction strategy provides the basis for the exceptional mechanical strength of these materials and for crucial physiological functions, such as structural support, defence and prey capture. For example, dragline silk fibres, that is, fibres produced by the major ampullate glands of spiders, serve as lifelines and are used for the construction of the outer rim and spokes of the orb web. They possess unparalleled mechanical properties with a unique combination of high tensile strength (1–2 GPa) and extensibility (50–60% strain at failure)[8] owing to the nanoconfinement and orientation of the silk nanofibrils. These mechanical features enable a silk fibre to absorb a large amount of energy before breaking; therefore, its toughness, which is the area under the stress–strain curve, is higher than that of steel and Kevlar fibres[8,11,12] (FIG. 2a). Trees can adjust the mechanical properties of wood to adapt to wind and to regulate tree growth, owing to the orientation of the laminar cellulose nanofibrils in the cell walls[10], and the 3D helicoidal stacking of chitin nanofibril layers enables exoskeletons to resist fracture through energy dissipation and limiting crack propagation[13].

The distinct structure–property–function relationships of such biological architectures can be explored for the design and fabrication of biopolymer-based, nanofibrillar materials. Compared with other biological nanomaterials, such as DNA, microfilaments or amyloid fibrils, which are challenging to produce on a large scale, cellulose, chitin and silk nanofibrils, which represent three of the most abundant biopolymer nanofibrils on Earth, have great potential for large-scale applications owing to the availability and easy production of the basic materials[5,14,15]. Cellulose nanofibrils and nanocrystals, that is, the crystal

domain of the cellulose nanofibril, have already been commercially produced[5]. The high mechanical performance, sustainability, availability, low-cost production, low weight and biocompatibility make nanofibrillar materials interesting for many applications[5,14–16], ranging from their use as nanofillers to reinforce composites and polymers[17,18] to the production of high-tech materials with specific performance demands[5,19–22]. Biopolymer nanofibrils can be manufactured into 0D materials (microspheres), 1D materials (fibres), 2D materials (membranes and nanopapers) and 3D materials (gels, foams, scaffolds and 3D-printed materials). Microspheres can be used as drug and cell carriers[23], fibres are investigated for the production of mechanically enhanced materials[24–36] and 2D materials can be fabricated as transparent, non-porous or composite multilayer membranes and as membranes with liquid crystal textures. These materials have been used for flexible optic and electronic devices[37,38], for water filtration[39], as substrates for batteries[40] and to improve the mechanical properties to provide fracture resistance to structural materials[41–43]. Gels, foams, scaffolds and 3D-printed constructions have broad applications, for example, in tissue engineering, as inorganic templates, for water–oil separation, to support cell adhesion and survival, and for mechanically enhanced bulk materials[5,14,15].

However, the structures and/or properties of most artificial biopolymer nanofibril-based materials remain inferior to their analogues found in nature. For example, the mechanical strength, elastic modulus and toughness of most cellulose, chitin and silk composites do not match those of natural materials composed of the same components[44]. How to design and optimize the structure–property–function relationships of biopolymer nanofibril-based materials remains a key question in the field. A major goal is to mimic multiscale construction strategies for the synthesis of artificial nanofibrillar materials and to provide a blueprint for the de novo design of features and functions that match or even exceed those of natural materials.

In this Review, we explore multiscale construction strategies found in nature, including nanoconfinement, nanofibril orientation and 3D helicoidal stacking, exemplified by the formation and mechanical properties of silk fibres, wood and exoskeletons. Rational design routes mimicking these biological multiscale construction strategies are then investigated for the development of synthetic nanofibril-based materials. Finally, we discuss challenges and directions for the development of next-generation biopolymer nanofibril materials.

Multiscale construction in nature

Nanoconfinement

Nanoconfinement describes the optimization of a specific material property, such as strength, stiffness or toughness, by confining the building blocks to a critical length scale[8,45]. In spider silk, nanoconfinement of the antiparallel β-sheets, representing the basic crystal unit, to 2–4 nm results in strong hydrogen bonding and consequent dissipative molecular stick–slip deformation of the fibre, which leads to higher strength, stiffness and toughness than in fibres built with nanocrystals of larger dimensions (FIG. 2b). During stick–slip shear motions, hydrogen bonds can reform, which increases the total dissipated energy and protects them from adverse exposure to the surrounding water (FIG. 2c). Above a critical length scale (4 nm in the case of spider silk[8]), the deformation mode of the

nanocrystal changes from a favourable shear mode to an unfavourable bending mode (FIG. 2d,e). In the bending mode, the non-uniform tensile deformation of the hydrogen bonds across the β-strand leads to their rupture and subsequent crack-like flaws. The cracks allow water molecules to enter the crystal regions under tension, which disrupts the crystal structure and causes catastrophic failure through brittle fracture. By contrast, the shear-governed deformation of smaller crystal units triggers a self-healing mechanism until complete rupture occurs (FIG. 2c).

Natural spider silk fibres often have defects, such as cavities, cracks or tears. These defects, which can reach several hundred nanometres in size[46], occur between the nanofibrils and can cause material failure through localized stress concentrations. Computer simulations using mesoscale spring models[47] have shown that a nanofibril length of about 50 ± 30 nm leads to increased strength and toughness at the macroscale because, at this length scale, protein domains synergistically resist deformation and failure and cracks do not have an impact on the mechanical response of the fibres. Natural silk materials are protected against defects through confinement of the nanofibril dimensions to approximately 20–80 nm (REFS 47,48).

Nanofibril orientation

Wood represents an outstanding example of how nature uses highly oriented nanofibrils to control mechanical anisotropy. Wood cell walls are composed of a single primary layer and three secondary layers (S_1, S_2 and S_3). The 4–5 μm-thick S_2 layer is the dominant component, composed of up to 95% (w/w) wood tracheids, that is, elongated cells of the plant water-transport system[2,49–53] (FIG. 3a). The stiff cellulose nanofibrils, which make up approximately 45% (w/w) of the S_2 layer, helically wind around these tube-like cells along the longitudinal cell axis[2,10], endowing wood cell walls with anisotropic mechanical properties that can be controlled by tuning the direction of the nanofibrils. The orientation of the cellulose nanofibrils is characterized by the microfibril angle (MFA; here, microfibril is the same as nanofibril)[50,51], which is defined as the angle between the nanofibril axis and the cell axis. In the S_2 layer, the MFA can vary between 0° and ~60°, which defines the anisotropy of the cell wall, similar to how the orientation of glass fibres controls the anisotropy of bulk fibre-reinforced polymers[2,54]. A strain causing an MFA of 45° results in a lower Young's modulus than a parallel strain (MFA = 0) owing to a change in compressive or tensile load distribution between the matrix components and the fibres[50,51] (FIG. 3a). Accordingly, the stress–strain curves of cell walls with a small MFA show brittle fracture with an almost full elastic response, whereas cell walls with a high MFA typically show tough biphasic or triphasic mechanical behaviour[55], with an elastic phase from zero strain to the yield point, that is, the stress at which the material begins to plastically deform, and a plastic deformation region beyond the yield point. Once the critical shear stress in the matrix is reached at the yield point, the matrix behaves as a viscous flow and the cellulose nanofibrils start gliding because of the stick–slip mechanism, which can be attributed to residual hydrogen bonds between the stiff cellulose nanofibrils and soft matrix components[56–58]. Thus, the distinct mechanical properties, for example, the tensile stiffness, of the different wood tissue types are defined by the MFAs in the respective cell walls (FIG. 3a). Interestingly, to compromise between bending flexibility and fracture or buckling

resistance, opposite cellulose nanofibril orientation strategies are found in young and mature trees[10]. In young trees, juvenile wood fibres with a large MFA form flexible trunks that can handle strong winds through bending and minimizing exposed areas. By contrast, in mature trees, wood fibres with small MFAs form stiff trunks, which are able to withstand wind loads[10,55,59].

3D helicoidal stacking

The 3D helicoid represents an important anisotropic biopolymer nanofibril architecture[60] (FIG. 1). In 3D helicoids, the nanofibrils are aligned as planar layers along their normal direction and helically stacked; adjacent layers are rotated by a constant angle, and the arrangement completes a full 180° rotation. Similar structures appear in chiral nematic (also referred to as cholesteric) textures. The 3D helicoid is a common structural motif in chitin nanofibril-based natural materials[1,61], such as the exoskeleton of arthropods (for example, crab, lobster and shrimp) or of insects[62,63], and has important effects on both the mechanical and optical properties of the material.

Improved fracture resistance.—Like the cellulose multi-layers in wood, helicoidal structures enable inplane mechanical anisotropy[3] and increase the fracture resistance of materials. The cuticle of lobster (*Homarus americanus*)[13] is a well-studied model, in which the chitin nanofibril orientation varies in different layers in order to withstand omnidirectional forces. Furthermore, such twisted chitin nanofibril layers provide increased toughness because the misaligned fibre planes enable multi-layer, rather than single-layer, crack propagation[13]. The helicoidal structure further increases the mechanical anisotropy and stiffens the material in the normal direction; the anisotropy ratio of the elastic modulus of the cuticle gradually changes from 4.25 (single-crystalline chitin) to 1.75 (mineralized chitin–protein nanofibrils) and 1.4 for the helicoidal structure[64]. In certain shrimp species, the highly mineralized chitin nanofibril helicoidal structures are additionally integrated with other mineral layers (for example, apatite nanocrystals), establishing a mechanical gradient in order to resist high-velocity impacts. For example, the hammer-like dactyl club of the peacock mantis shrimp (*Odontodactylus scyllarus*) generates high-velocity blows that can reach accelerations of $>10^5$ m s^{-2} and speeds of 23 m s^{-1}, generating forces of up to 1,500 N (REFS 65–67) (FIG. 3b). The dactyl strike is recognized as one of the fastest and most powerful impacts in nature and can crack tough biological composites, such as mollusc shells; however, the dactyl club remains intact owing to the mechanical gradient structure, which can be divided into two distinct regions: the impact region and the periodic region[65,68]. The impact region consists of an impact surface (hard external zone)[68] and a herringbone structure region[68], which features a highly ordered, compact and pitch-graded sinusoidal arrangement (the amplitude is graded in the radial direction) of helicoidally arranged chitin nanofibrils covered with mineralized hydroxyapatite, which is oriented parallel to the long axis of the chitin nanofibrils (FIG. 3b). This structural design endows the impact region with quasi-plastic behaviour and an anisotropic stiffness response[69], enabling stress redistribution and out-of-plane stiffness (that is, the stiffness along the *x* direction of the herringbone pattern) in response to compressive loading. The (inner) periodic region features a partially mineralized chitin nanofibril helicoidal structure, which acts as the primary energy-absorbing layer. The integration of soft chitin nanofibrils with stiff

nanominerals causes an elastic modulus mismatch in the impact region, leading to crack deflection near the impact surface[65]. Helicoidal structures are also able to dissipate the released energy through the propagation (twisting) of microcracks, increasing the essential work of fracture, that is, the absorbed energy required to propagate a crack. The incorporation of sinusoidal interfaces in the herringbone structure further increases the toughness of the dactyl club by extending the path length during crack growth. The combination of a stiff and hard exterior with a tough and energy-absorbent core makes the dactyl club tolerant to damage and capable of with-standing thousands of repeated impact events without catastrophic failure[70,71].

Structural colour.—In some insects (for example, *Chrysina aurigans* (scarabs)[72] or *Buprestoidea* (jewelled beetles)[73]) and plants (for example, rainforest understorey plants[74] or the epicarp of *Pollia condensata* (marble berry)[75]), transparent chitin or cellulose nanofibril-based helicoidal structures enable the production of structural colour (FIG. 3c). Such structural colourations play a role in many biological functions, such as mating, signalling and camouflage[74]. Similar to nematic liquid crystals[76,77], the optical properties of helicoids are defined by two structural parameters[74]: the distance between two planes with the same fibril orientation (pitch, p) and the handedness of the helix. Only circularly polarized light of the same chirality (handedness) as the helicoid is reflected by helicoidal structures, whereas light with opposite chirality is transmitted (FIG. 3c). Of note, this is a different mechanism than how circularly polarized light is reflected by a plane mirror; in this case, a 180° phase shift of the light upon reflection results in a change of handedness. Assuming that the difference between the refractive index of the biopolymer nanofibrils and that of the matrix in which they are dispersed is low, the maximal wavelength, λ_{max}, of light reflected by the helicoid can be calculated by[78]:

$$\lambda_{max} = 2 \times p \times n_{avg} \quad (1)$$

in which n_{avg} is the average refractive index of the biopolymer nanofibrils and p is the pitch. Therefore, if $p/2$ corresponds to a wavelength of visible light (400–700nm), the material features structural colour[22].

Fabrication strategies

Notably, 1D, 2D and 3D manufacturing techniques can be applied to recreate the structure and orientation of biopolymer-based nanofibrils. Artificial spinning techniques are useful to regulate nanofibril orientation in 1D, whereas the organization of fibrils in planes can be achieved through chemical modification (for example, non-covalent surface modification, sulfonation, 2,2,6,6-tetramethylpyperidine-1-oxyl (TEMPO)-mediated oxidation or esterification)[79], by applying electric fields[80] or magnetic fields[81] and through spray-assisted layer-by-layer assembly[82]. Furthermore, 2D materials, such as membranes and nanopapers, can be used as flexible optical and/or electrical substrates, replacing traditional materials, such as silicon dioxide, because of their transparency, superior biodegradability and deformability[37,38]. Biopolymer nanofibrils can be further combined with inorganic nanomaterials, such as nanoclays[41,42], graphene oxide or graphene[43], to build hybrid nacre-like nanopapers. Owing to their highly ordered brick-and-mortar structure, these nanopapers

are tougher and/or stronger than materials made by the individual components. The fabrication of 3D nanofibrillar architectures remains challenging. However, advances in 3D printing technologies have enabled the production of highly ordered biopolymer nanofibril arrangements.

Artificial spinning

Wet spinning.—Wet spinning is commonly used to control the orientation of biopolymer nanofibrils in fibres. In this process, a spinning dope is extruded through a spinneret into a non-solvent coagulation bath, in which the dope solidifies into a fibre through precipitation. Through this method, dispersions or gels of biopolymer nanofibrils, including silk[24], cellulose[25,28–32] and chitin nanofibrils[26,27], can be spun into oriented fibres with diameters ranging from several to hundreds of micrometres and lengths up to several metres. The alignment of the fibres is defined by the flow regime and the dehydration of the fibre precursors before, during and after extrusion through the long and narrow spinneret, which has an important impact on the orientation and alignment of the nanofibrils. After passing through the nozzle, the orientation and alignment of the nanofibrils in the fibre can be fixed through solvent depletion during coagulation and dehydration. However, the interactions between the fibres, which are caused by dehydration and which determine their orientation, can be weak; thus, post-processing, such as post-drawing and steam annealing, can be applied to fix the orientation and structure of the nanofibrils.

Dry spinning.—Dry spinning mimics the natural spinning of silk by spiders[33,34]. The silk dope is solidified to a fibre immediately upon leaving the spinneret owing to the evaporation of a volatile solvent; there are no additional immobilization or post-processing steps required. The dry spinning process generates highly oriented biopolymer nanofibril-based fibres and is facile and environmentally friendly compared with wet spinning. As in the wet spinning process, the nanofibrils are oriented because of the shear force generated by the extrusion or reeling process. Thus, the orientation is tunable through changing the extrusion and/or reeling speed, as well as through optimizing the spinning device and spinneret geometries. Moreover, in contrast with wet spinning processes, in which the nanofibrils can be oriented only along the fibre axis, dry spinning can generate a polymorphic arrangement of biopolymer nanofibrils in a single fibre[34]. For instance, yarn-like spiral fibres can be spun through rotation of the collector on a plane perpendicular to the fibre axis[34]. Sponge-like or tendril-like helical fibres can be produced through extrusion of the spinning solution onto a cylindrical collector[34]. However, dry spinning requires higher dope concentrations than wet spinning to ensure continuous spinning so that the as spun fibres do not collapse or break. For example, the minimal solid content of unmodified cellulose nanofibrils necessary for wet spinning is 1.47%, whereas 3% is required for dry spinning[25]. The minimal content of a silk microfibril dope required for spinning is even higher (>4%)[34]. Of note, it is difficult to quantify and compare the minimal spinnable solid content because it correlates with various other factors, such as the device setup, the spinning conditions and the source, size, shape and pretreatment of the biopolymer nanofibrils.

Wet spinning and dry spinning are efficient techniques to fabricate aligned fibres from elongated nanofibril systems. However, the mechanical properties of these fibres are inferior

to those of natural fibres with the same components (FIG. 4a). The highest specific elastic modulus and strength of cellulose nanofibril-based fibres achieved by wet spinning were ~22 GPa (REF. 26) and ~206 MPa (REF. 29), respectively, which are less than those of natural cellulose nanofibril-based fibres; for example, the plant Ramie (*Boehmeria nivea*) has a specific modulus and strength of 42 GPa and 613 MPa, respectively[83] (FIG. 4b). This gap in mechanical properties between natural and artificial fibres has motivated the design of more ingenious spinning processes and devices to tailor nanofibril orientation and thus mechanical performance. Plotting the strength versus the elastic modulus of fibres with different orientation indices (or order parameters), which is an important quantitative parameter to define nanofibril orientation, reveals that both the strength and the elastic modulus increase with higher orientation index (FIG. 4c). Therefore, regulation of biopolymer nanofibril alignment provides a possible tool to further improve the mechanical properties.

Microfluidic spinning.—Microfluidic spinning is a promising technique to regulate biopolymer nanofibril assembly and to improve the mechanical properties of the fibres. An inherent advantage of microfluidics is that the spinning channel can be designed in a way to control the dope flow and to optimize the processing parameters. In addition, pH and salt gradients, as well as shear flow, can be introduced in the microfluidic channel by the use of double concentric channels to modulate the mechanical properties of the fibres[84,85]. For example, a flow-focusing spinning system can be used to control the alignment of cellulose nanofibrils or nanocrystals and to produce high-performance cellulose nanofibril-based fibres[35,36] (FIG. 4d). The cellulose nanofibril orientation along the filament direction is defined by regulation of the processing parameters, such as flow rate, flow acceleration and ionic strength. Therefore, the mechanical properties of the regenerated cellulose nanofibril-based fibres can be substantially improved.

The specific ultimate strength is approximately 490 MPa, which is much higher than that of fibres produced by dry spinning (~198 MPa) or wet spinning (~275 MPa) techniques[35] (FIG. 4a). Moreover, the fibres spun from cellulose nanofibril and/or recombinant spider silk protein dopes possess exceptional mechanical properties[36]; the stiffness, strength and toughness reach approximately 55 GPa, 1,015 GPa and 55 MJ m^{-3}, respectively, which are higher than those of previously reported regenerated biopolymer fibres[36] and most natural cellulose nanofibril-based fibres[55]. However, the elastic moduli of single cellulose nanocrystals (100–160 GPa (REF. 86)) and cellulose nanofibrils (~100 GPa (REF. 21)) are stronger than those of fibres fabricated by microfluidic spinning. Despite important improvements in the fabrication of synthetic fibres, an ideal spinning technique remains elusive. Although microfluidic-based spinning can be used to produce fibres with desirable mechanical performance, the process is complicated and scale up is challenging. Alternatively, pattern moulding[87] can be applied to fabricate centimetre-scale channels with sophisticated geometric constraints, such as anchors, cables, lattices and webs[87] (FIG. 5a), which can be used to direct the orientation of nanofibrils and to generate gradients of silk nanofibrils in materials through shear flow and force extension. Therefore, pre-designed internal structures can be manufactured for the engineering of materials with specific mechanical properties.

The strength and elastic modulus of biopolymer nanofibril-based fibres in the wet state are usually substantially lower than those in the dry state[30]. Thus, the fibres need to be post-processed to be able to resist water or moisture. Coating[28] and crosslinking techniques[32] have been developed to improve the stability of biopolymer nanofibril fibres against moisture uptake. In addition, the source, size and shape of biopolymer nanofibrils have a crucial effect on the spinning process and fibre properties. Stress–strain curves of different biopolymer nanofibril-based regenerated fibres show that fibres produced from silk and chitin nanofibrils possess higher strain to failure values than cellulose nanofibril fibres. However, regenerated cellulose-based fibres are stronger and stiffer than silk and chitin-based fibres (FIG. 4a). Therefore, the development of multicomponent dopes, by combining the different base materials, may provide a promising strategy for the production of fibres with optimal strength, stiffness and toughness. However, the nanoconfinement and interfacial interactions of such regenerated fibres remain to be optimized.

3D printing

Advances in 3D printing technologies, especially in direct ink writing techniques, have enabled the use of biopolymer nanofibril-based inks to generate 3D architectures with highly ordered nanofibril arrangements[88–95] (FIG. 5b). Biopolymer nanofibril-based inks can be equipped with suitable rheological properties through the design of non-Newtonian viscoelastic solutions that feature shear-thinning behaviour; that is, the viscosity decreases under shear strain. Nanofibrils with low aspect ratios (for example, cellulose nanocrystals or chitin nanowhiskers) are good candidates because of the absence of physical entanglements and the high nanofibril concentration. For example, shear-thinning behaviour is observed in aqueous inks with high concentrations of cellulose nanocrystals (10–20% (w/v)) without the need to add rheological modifiers. However, cellulose nanofibril solutions usually have a low solid content (0.8–2.5% (w/v)) because of the entangled state of high-concentration cellulose nanofibril suspensions and thus cannot be used as inks for direct ink writing. To address this issue, the rheological properties of cellulose nanofibril-based inks can be modified through the addition of thickening agents, for example, alginate, fumed silica[93], laponite[84], graphene oxide[94] and polymers[92]. By applying this strategy, complex 3D architectures, such as ear-like[95], chair-like[91] or lattice cell-like structures[92], can be printed using biopolymer nanofibril-based inks. Inspired by biological actuation systems, such as scales, chiral pod pericarps and specific petals, which enable certain plant tissues (for example, pine cones, pea pods and orchid flowers[54,96–103]) to dynamically adapt to environmental changes, such as humidity, cellulose nanofibril ink-based 3D printing has been applied to encode localized, anisotropic swelling behaviour through regulation of the site-specific orientation of the cellulose nanofibrils[90] (FIG. 5b). These materials can bend, fold and change shape in response to changes in the surrounding humidity.

Artificial chiral nematic films and droplets

In suspensions of silk, cellulose or chitin nanocrystals or whiskers, the rod-like nanocrystals assemble into liquid crystalline structures with left-handed chiral nematic behaviour at concentrations ≥1–7% (w/v)[104–108]. The nanocrystal suspensions retain their chiral nematic order in the dry state and assemble into helicoidal structures, forming thin solid films[20,22,107–114] (FIG. 6a). These chiral nematic films exhibit the same structural features

as natural helicoids and can act as photonic structures, selectively reflecting circularly polarized light at a wavelength matching the helicoidal pitch *p*, according to equation 1. Therefore, by controlling the *p* of the chiral nematic film, the wavelength of the light can be shifted to tailor the reflected colour. This can be achieved by controlling the film formation processes. For example, pre-ultrasonication of the nanocrystal suspension triggers a redshift, and an increase in the ionic strength results in a blueshift. The temperature at which the film is dried also affects the reflected colour, with a high temperature usually leading to a blueshift. Applying electric[115–117] or magnetic fields[118] during film formation, or adding organic molecules or polymers[119–121] can also trigger a wavelength shift of the reflected light.

The chiral nematic structure of cellulose or chitin nanocrystal-based materials can further serve as a scaffold for the fabrication of functional mesoporous films. Chiral nematic films can be directly transferred onto polymer-based[119–123], silica-based or organosilica-based[124–126] composite films, and the cellulose nanocrystal template can then be selectively removed through alkaline treatment (for polymers) or high-temperature sintering (for silica-based systems) (FIG. 6b). Owing to their iridescent, mesoporous and flexible features, these (organo)silica films can be used as sensors and reflectors[20]. Alternatively, the films can be further transferred onto other chiral materials, such as highly porous semiconducting carbon films[127] or titanium dioxide-doped[128], gold-doped[129] or silver-doped silica films[130]. This approach opens up new routes for the engineering of liquid crystalline materials. The pitch and thus the structural colour can be controlled through changing the degree of swelling, which allows for the design of mesoporous polymers with a series of swelling ratios and therefore a variety of colours. The swelling of the materials and the related colour changes depend on the polarity of the solvent, which makes these materials interesting candidates for applications as solvent sensors[122] (FIG. 6b). The 3D chiral nematic structures of biopolymer nanofibril-based materials are still difficult to produce131 because, in bulk materials such as hydrogels or foams, the pitch is usually larger than the wavelength of visible light. Furthermore, the solubilization and functionalization of chitin nanowhiskers without sacrificing their liquid crystal textures have proved difficult[107].

The topology has an important effect on the self-assembly and properties of biopolymer nanofibril liquid crystals[132–135], because structural constraints break the morphological symmetry of an architecture (FIG. 6c). Spherical topologies, such as droplets or thin liquid shells, are characterized by isotropic confinements and curvature, causing topological structural defects, such as radial declinations and dislocations[35]. Confined droplets can be prepared by solvent stabilization[134], emulsification[135] and microfluidics-assisted techniques[132,133] (FIG. 6d). Solvent stabilization[134] and emulsification[135] are simple and scalable, but the homogeneity of the microspheres is difficult to control. Droplet-based microfluidics[132,133] can be applied to produce homogeneous microspheres at the cost of scalability. Alternatively, the bottom-up self-assembly[23] of biopolymers can address issues with homogeneity and scalability. Investigating topological constraints is a useful tool to study particle packing, the anisotropic self-assembly of biopolymer nanofibrils and the relaxation of colloidal liquids (FIG. 6e). Additionally, confined droplets can be used for the fabrication of functional materials; for example, confined microspheres can act as a template for nanoparticles[133], such as polymers, metals, carbon or metal oxide nanocolloids, to

control nanoparticle partitioning in the isotropic core (topological defect) and the chiral nematic shell in order to form chiral nematic cellulose nanocrystal droplets. The co-assembly of cellulose nanocrystals with polymers and inorganic nanoparticles endows the droplets with plasmonic, fluorescent and magnetic properties, which can be explored for the design of stimuli-responsive liquid crystalline materials[133]. However, like every microsphere preparation method, emulsification[135] and bottom-up self-assembly[23] suffer from microsphere redispersion in aqueous solution, which needs to be considered, especially for applications in drug delivery and as cell carriers[23].

Rational material design

The creation of synthetic materials that mimic the optical and mechanical properties of natural nanofibrillar structures has been hampered by the inability to fabricate biopolymer-based fibres with features equal to those found in nature. Materiomics copies the multiscale fabrication strategy of natural nanofibrils by applying a rational material design approach; the fundamental structure–process–property relationships are examined through the iterative integration of computational modelling with experimental fabrication[136], which allows for the in silico design of material preparation protocols and properties. Multiscale modelling combines and links computational spatiotemporal hierarchies, offering a toolkit to optimize the structure and predict the properties of a material in silico at different timescales and length scales, ranging from the atomic (Å) to the metre scale[137] (FIG. 7). The different levels of interactions and the hierarchical assembly of natural and artificial biopolymer nanofibril-based materials can be either individually or concurrently analysed, and the data derived from these ‘virtual’ materials inform the experimental synthesis. The structure and properties of the synthesized materials can be characterized at different scales and spatial resolutions by applying experimental and theoretical methods (FIG. 7a). These data can then be used for the validation and optimization of the computational and theoretical models (FIG. 7b,c). This multicycle and multiscale optimization approach enables the prediction of the structure, properties and functions of a material, without the need for multiple trial-and-error experiments (FIG. 7c).

Such de novo computational strategies have been applied for the synthesis of functional proteins[138,139] and peptide and protein nanofibrils (for example, amyloid fibrils[140–142]); however, they are not yet commonly used for the design of biopolymer nanofibril-based materials. Silk-based and collagen-based materials[143] have been fabricated through integrating mesoscopic modelling with genetic block copolymer synthesis. Using this approach, a series of silk-based materials (that is, fibres and hydrogels) with specific mechanical and chemical properties have been designed and fabricated[144–147]. Materiomics can also be applied for the design of the mesostructure of biopolymer nanofibril-based materials, for example, for the fabrication of multilayer structures that can be used as water filtration membranes. These membranes require optimal multilayer architectures to enable increased water throughput, filter efficiency and molecular loading capacity[39,148,149], which are experimentally challenging to prepare. Comparative computational simulations revealed that weak interactions between protein nanofibrils and calcium nanomineral plates cause the assembly of highly ordered multilayer nanoporous membranes, which was experimentally confirmed by mixing silk nanofibrils with hydroxyapatite[39]. These membranes are

characterized by ultrafast water penetration and efficient removal of contaminants, including heavy metal ions, dyes and proteins. Rational design by materiomics increases the design space for materials and allows for the creation and fabrication of nanofibrillar materials with specific structures and properties.

Conclusions and outlook

Cellulose, chitin and silk possess remarkable mechanical and optical properties and therefore are of great interest for the fabrication of functional and versatile materials. The superior mechanical properties can be mainly attributed to the hierarchical structural composition of these nanofibrillar materials, which is challenging to recreate experimentally. Therefore, rational material design strategies are required to mimic the assembly and thus function of natural nanofibrillar structures with the goal to engineer performance-optimized biopolymer materials.

Engineering approaches to recreate the nanoscale architecture of biopolymer materials typically involve the dissolution of the natural biopolymer (to obtain individual polymer chains) and the consequent regeneration into specific material formats through processes such as spinning, casting, moulding or freeze drying. However, these materials do not exhibit the desired well-designed and highly organized nanostructures of native biopolymer systems. The self-assembly into nanofibrillar structures rather than the natural structures of the individual components plays a key role in the mechanical performance and optical chirality of these materials. For example, the toughness of fabricated silk nanofibril membrane is $(5 \pm 2) \times 10^5$ J m^{-3}, which is more than 100 times smaller than that of silk fibres produced by the silkworm (*Bombyx mori*)[6,147]; the Young's modulus of engineered cellulose nanofibril membranes is approximately 6 GPa (REF. 150), which is about five times less than that of hardwood fibres[55]. Therefore, processes that enable biomimetic reassembly into macroscopic architectures need to be developed and optimized to recreate the properties of natural nanofibrillar-based fibres for the fabrication of optical, biomedical and environmentally adaptive materials. Nature has created a set of general design rules to form functional nanofibrillar materials, including nanoconfinement, fibrillar orientation and highly ordered 2D and 3D constructions[7–9,10], established through assembly processes in aqueous solution at ambient temperature and pressure. However, conventional engineering approaches usually do not exploit self-assembly as the main driving force, tend to be more energy intensive and often require the use of toxic agents. Strategies mimicking nature's multiscale assembly routes could offer a possible route to recreate the properties and functions of natural fibrillar materials.

Multiscale, rational material design can be applied to optimize structure–property–function relationships through the creation of hierarchical structures. At the molecular scale, the chemical structure, molecular weight, functional groups and hydrophobic or hydrophilic partitioning can be tailored on the basis of full-atomic or coarse-grained molecular dynamics modelling, which can predict nanofibrillar formation and assembly a priori. At the mesoscopic and macroscopic levels, the mechanical and optical performance, as well as the dynamic stimuli response, of nanofibrillar materials can be designed by the synergistic integration of multiscale modelling and experimental manufacturing (such as spinning, film

casting and 3D printing). Therefore, anisotropic nanofibril arrangements can be introduced and gradients can be incorporated to endow materials with mechanical strength and flexibility and to support dynamic interactions with environmental stimuli (for example, humidity, temperature or light)[17,102]. Moreover, multiscale coarse-grained modelling can be used to predict the deformation behaviour of architectures with distinct nanofibril arrangements, and 3D printing can be applied to build such optimized structures through site-specific printing[90]. This rational approach can be applied at all stages of the material design process, from sequence design to macroscopic fabrication.

However, computational challenges remain for the broad implementation of rational material design strategies for the fabrication of nanofibrillar structures. For example, developing more precise modelling toolkits, such as force fields, algorithms and theories, will improve the prediction of specific functional outcomes. High-throughput computational screening and machine learning[151] may provide an effective route to improve the validation of nanofibrillar screening. Nature typically creates structures through mechanisms of growth, which can be a slow process that occurs over months or years and is thus not suitable for commercial production. Engineering approaches need to accelerate the material assembly process without undermining the green and environmentally friendly features of biopolymer nanofibrils. Therefore, detailed cradle to grave life cycle assessments of the different fabrication methods are needed to address economic and scientific issues related to production and application[152–154]. Further insight into the structure–property–function relationships of natural materials will certainly spark the development of bioinspired and biomimetic strategies for the economically beneficial and energy-efficient design of novel biopolymer nanofibril-based functional materials. These insights can be achieved through the synergistic integration of multiscale modelling with advanced static and dynamic characterization techniques, including electron microscopy, synchrotron light sources and ultrafast spectroscopies.

Acknowledgements

The authors acknowledge the students and colleagues who have worked with us over the years on research projects related to the theme of this Review. The authors also acknowledge the US National Institutes of Health (NIH) (U01EB014976, R01DE016525), the Air Force Office of Scientific Research (FA8650-16C-5020) and the Office of Naval Research (ONR) (N000141612333) for their support of studies related to the topic of this Review. S.L. acknowledges a starting grant given by ShanghaiTech University.

References

1. Neville AC Biology of Fibrous Composites: Development Beyond the Cell Membrane (Cambridge Univ. Press, New York, 1993).
2. Meyers MA & Chen PY in Biological Materials Science: Biological Materials, Bioinspired Materials, and Biomaterials 53–97 (Cambridge Univ. Press, Cambridge, 2014).
3. Mitov M Cholesteric liquid crystals in living matter. Soft Matter 13, 4176–4209 (2017). [PubMed: 28589190]
4. Gibson LJ The hierarchical structure and mechanics of plant materials. J. R. Soc. Interface 9, 2749–2766 (2012). [PubMed: 22874093]
5. Moon RJ, Martini A, Nairn J, Simonsen J & Youngblood J Cellulose nanomaterials review: structure, properties and nanocomposites. Chem. Soc. Rev 40, 3941–3994 (2011). [PubMed: 21566801]

6. Bidhendi AJ & Geitmann A Relating the mechanics of the primary plant cell wall to morphogenesis. J. Exp. Bot 67, 449–461 (2016). [PubMed: 26689854]
7. Giesa T & Buehler MJ Nanoconfinement and the strength of biopolymers. Annu. Rev. Biophys 42, 651–673 (2013). [PubMed: 23654307]
8. Keten S, Xu ZP, Ihle B & Buehler MJ Nanoconfinement controls stiffness, strength and mechanical toughness of β sheet crystals in silk. Nat. Mater 9, 359–367 (2010). [PubMed: 20228820] This paper introduces the nanoconfinement of silk nanocrystals.
9. Giesa T, Pugno NM, Wong JY, Kaplan DL & Buehler MJ What's inside the box? – length-scales that govern fracture processes of polymer fibers. Adv. Mater 26, 412–417 (2014). [PubMed: 24431127]
10. Fratzl P & Weinkamer R Nature's hierarchical materials. Prog. Mater. Sci 52, 1263–1334 (2007).
11. Fu CJ, Shao ZZ & Fritz V Animal silks: their structures, properties and artificial production. Chem. Commun. 6515–6529 (2009).
12. Cranford SW, Tarakanova A, Pugno NM & Buehler MJ Nonlinear material behaviour of spider silk yields robust webs. Nature 482, 72–76 (2012). [PubMed: 22297972]
13. Naleway SE, Porter MM, McKittrick J & Meyers MA Structural design elements in biological materials: application to bioinspiration. Adv. Mater 27, 5455–5476 (2015). [PubMed: 26305858]
14. Omenetto FG & Kaplan DL New opportunities for an ancient material. Science 329, 528–531 (2010). [PubMed: 20671180]
15. Ravi Kumar MNV A review of chitin and chitosan applications. React. Funct. Polym 46, 1–27 (2000).
16. Wang S, Lu A & Zhang L Recent advances in regenerated cellulose materials. Prog. Polym. Sci 53, 169–206 (2016).
17. Capadona JR, Shanmuganathan K, Tyler DJ, Rowan SJ & Weder C Stimuli-responsive polymer nanocomposites inspired by the sea cucumber dermis. Science 319, 1370–1374 (2008). [PubMed: 18323449]
18. Capadona JR et al. A versatile approach for the processing of polymer nanocomposites with self-assembled nanofibre templates. Nat. Nanotechnol 2, 765–769 (2007). [PubMed: 18654428]
19. De France KJ, Hoare T & Cranston ED Review of hydrogels and aerogels containing nanocellulose. Chem. Mater 29, 4609–4631 (2017).
20. Kelly JA, Giese M, Shopsowitz KE, Hamad WY & MacLachlan MJ The development of chiral nematic mesoporous materials. Acc. Chem. Res 47, 1088–1096 (2014). [PubMed: 24694253]
21. Dufresne A Nanocellulose: a new ageless bionanomaterial. Mater. Today 16, 220–227 (2013).
22. Giese M, Blusch LK, Khan MK & MacLachlan MJ Functional materials from cellulose-derived liquid-crystal templates. Angew. Chem. Int. Ed 54, 2888–2910 (2015).
23. Duan B et al. Highly biocompatible nanofibrous microspheres self-assembled from chitin in NaOH/urea aqueous solution as cell carriers. Angew. Chem. Int. Ed 54, 5152–5156 (2015).
24. Ling S et al. Integration of stiff graphene and tough silk for the design and fabrication of versatile electronic materials. Adv. Funct. Mater 28, 1705291 (2018). [PubMed: 30505261]
25. Lundahl MJ, Klar V, Wang L, Ago M & Rojas OJ Spinning of cellulose nanofibrils into filaments: a review. Ind. Eng. Chem. Res 56, 8–19 (2017).
26. Torres-Rendon JG, Schacher FH, Ifuku S & Walther A Mechanical performance of macrofibers of cellulose and chitin nanofibrils aligned by wet-stretching: a critical comparison. Biomacromolecules 15, 2709–2717 (2014). [PubMed: 24947934]
27. Das P et al. Tough and catalytically active hybrid biofibers wet-spun from nanochitin hydrogels. Biomacromolecules 13, 4205–4212 (2012). [PubMed: 23102411]
28. Walther A, Timonen JVI, Díez I, Laukkanen A & Ikkala O Multifunctional high-performance biofibers based on wet-extrusion of renewable native cellulose nanofibrils. Adv. Mater 23, 2924–2928 (2011). [PubMed: 21567482]
29. Iwamoto S, Isogai A & Iwata T Structure and mechanical properties of wet-spun fibers made from natural cellulose nanofibers. Biomacromolecules 12, 831–836 (2011). [PubMed: 21302950]
30. Lundahl MJ et al. Strength and water interactions of cellulose I filaments wet-spun from cellulose nanofibril hydrogels. Sci. Rep 6, 30695 (2016). [PubMed: 27465828]

31. Li Y et al. Hybridizing wood cellulose and graphene oxide toward high-performance fibers. NPG Asia Mater. 7, e150 (2015).
32. Mertaniemi H et al. Human stem cell decorated nanocellulose threads for biomedical applications. Biomaterials 82, 208–220 (2016). [PubMed: 26763735]
33. Hooshmand S, Aitomäki Y, Norberg N, Mathew AP & Oksman K Dry-spun single-filament fibers comprising solely cellulose nanofibers from bioresidue. ACS Appl. Mater. Interfaces 7, 13022–13028 (2015). [PubMed: 26017287]
34. Ling S et al. Polymorphic regenerated silk fibers assembled through bioinspired spinning. Nat. Commun 8, 1387 (2017). [PubMed: 29123097] This paper describes improved dry spinning techniques for producing polymorphic and mechanically enhanced regenerated silk fibres.
35. Håkansson KMO et al. Hydrodynamic alignment and assembly of nanofibrils resulting in strong cellulose filaments. Nat. Commun 5, 4018 (2014). [PubMed: 24887005]
36. Mittal N et al. Ultrastrong and bioactive nanostructured bio-based composites. ACS Nano 11, 5148–5159 (2017). [PubMed: 28475843] This paper demonstrates a microfluidic spinning method to obtain ultrastrong cellulose nanofibril-based regenerated fibres.
37. Ji S et al. High dielectric performances of flexible and transparent cellulose hybrid films controlled by multidimensional metal nanostructures. Adv. Mater 29, 1700538 (2017).
38. Zhu H et al. Extreme light management in mesoporous wood cellulose paper for optoelectronics. ACS Nano 10, 1369–1377 (2016). [PubMed: 26673796]
39. Ling S et al. Design and function of biomimetic multilayer water purification membranes. Sci. Adv 3, 1601939 (2017).This paper introduces a rational material design strategy to fabricate high-performance water purification membranes.
40. Kim JK et al. Hierarchical chitin fibers with aligned nanofibrillar architectures: A nonwoven-mat separator for lithium metal batteries. ACS Nano 11, 6114–6121 (2017). [PubMed: 28505417]
41. Jin H et al. Ionically interacting nanoclay and nanofibrillated cellulose lead to tough bulk nanocomposites in compression by forced self-assembly. J. Mater. Chem. B 1, 835–840 (2013). [PubMed: 32260742]
42. Liu Y, Yu SH & Bergström L Transparent and flexible nacre-like hybrid films of aminoclays and carboxylated cellulose nanofibrils. Adv. Funct. Mater 10.1002/adfm.201703277 (2017).
43. Shahzadi K et al. Reduced graphene oxide/alumina, a good accelerant for cellulose-based artificial nacre with excellent mechanical, barrier, and conductive properties. ACS Nano 11, 5717–5725 (2017). [PubMed: 28586191]
44. Egan P, Sinko R, LeDuc PR & Keten S The role of mechanics in biological and bio-inspired systems. Nat. Commun 6, 7418 (2015). [PubMed: 26145480]
45. Nova A, Keten S, Pugno NM, Redaelli A & Buehler MJ Molecular and nanostructural mechanisms of deformation, strength and toughness of spider silk fibrils. Nano Lett. 10, 2626–2634 (2010). [PubMed: 20518518]
46. Frische S, Maunsbach AB & Vollrath F Elongate cavities and skin–core structure in Nephila spider silk observed by electron microscopy. J. Microsc 189, 64–70 (1998).
47. Pilate G et al. Lignification and tension wood. C. R. Biol 327, 889–901 (2004). [PubMed: 15587080]
48. Du N et al. Design of superior spider silk: From nanostructure to mechanical properties. Biophys. J 91, 4528–4535 (2006). [PubMed: 16950851]
49. Déjardin A et al. Wood formation in Angiosperms. C. R. Biol 333, 325–334 (2010). [PubMed: 20371107]
50. Altaner CM & Jarvis MC Modelling polymer interactions of the ‘molecular Velcro’ type in wood under mechanical stress. J. Theor. Biol 253, 434–445 (2008). [PubMed: 18485371]
51. Fratzl P, Burgert I & Keckes J Mechanical model for the deformation of the wood cell wall. Z. Metallkd 95, 579–584 (2004).
52. Joseleau JP, Imai T, Kuroda K & Ruel K Detection in situ and characterization of lignin in the Glayer of tension wood fibres of Populus deltoides. Planta 219, 338–345 (2004). [PubMed: 15067547]

53. Eder M, Arnould O, Dunlop JWC, Hornatowska J & Salmén L Experimental micromechanical characterisation of wood cell walls. Wood Sci. Technol 47, 163–182 (2013).
54. Fratzl P & Barth FG Biomaterial systems for mechanosensing and actuation. Nature 462, 442–448 (2009). [PubMed: 19940914]
55. Stevens C Industrial Applications of Natural Fibres: Structure, Properties and Technical Applications. Vol. 10 (John Wiley & Sons, 2010).
56. Keckes J et al. Cell-wall recovery after irreversible deformation of wood. Nat. Mater 2, 810–813 (2003). [PubMed: 14625541]
57. Adler DC & Buehler MJ Mesoscale mechanics of wood cell walls under axial strain. Soft Matter 9, 7138–7144 (2013).
58. Jin K, Qin Z & Buehler MJ Molecular deformation mechanisms of the wood cell wall material. J. Mech. Behav. Biomed. Mater 42, 198–206 (2015). [PubMed: 25498207]
59. Burgert I in Materials Design Inspired by Nature: Function Through Inner Architecture (eds Fratzl P, Dunlop JWC & Weinkamer R) 128–150 (The Royal Society of Chemistry, Dorchester, 2013).
60. Bouligand Y Twisted fibrous arrangements in biological materials and cholesteric mesophases. Tissue Cell 4, 189–217 (1972). [PubMed: 4600349]
61. Neville AC Biology of the Arthropod Cuticle (Springer Science & Business Media, Berlin, 1975).
62. Fabritius HO et al. Functional adaptation of crustacean exoskeletal elements through structural and compositional diversity: a combined experimental and theoretical study. Bioinspir. Biomim 11, 055006 (2016). [PubMed: 27609556]
63. Raabe D, Sachs C & Romano P The crustacean exoskeleton as an example of a structurally and mechanically graded biological nanocomposite material. Acta Mater. 53, 4281–4292 (2005).
64. Nikolov S et al. Revealing the Design Principles of High-performance biological composites using ab initio and multiscale simulations: the example of lobster cuticle. Adv. Mater 22, 519–526 (2010). [PubMed: 20217746]
65. Weaver JC et al. The stomatopod dactyl club: a formidable damage-tolerant biological hammer. Science 336, 1275–1280 (2012). [PubMed: 22679090] This paper presents the exceptional damage tolerance mechanism of the stomatopod dactyl club.
66. Patek SN, Korff WL & Caldwell RL Biomechanics: Deadly strike mechanism of a mantis shrimp. Nature 428, 819–820 (2004). [PubMed: 15103366]
67. Patek SN & Caldwell RL Extreme impact and cavitation forces of a biological hammer: strike forces of the peacock mantis shrimp *Odontodactylus scyllarus*. J. Exp. Biol 208, 3655–3664 (2005). [PubMed: 16169943]
68. Yaraghi NA et al. A sinusoidally architected helicoidal biocomposite. Adv. Mater 28, 6835–6844 (2016). [PubMed: 27238289]
69. Amini S, Tadayon M, Idapalapati S & Miserez A The role of quasi-plasticity in the extreme contact damage tolerance of the stomatopod dactyl club. Nat. Mater 14, 943–950 (2015). [PubMed: 26053761]
70. Grunenfelder LK et al. Bio-inspired impact-resistant composites. Acta Biomater 10, 3997–4008 (2014). [PubMed: 24681369]
71. Liu Z, Meyers MA, Zhang Z & Ritchie RO Functional gradients and heterogeneities in biological materials: design principles, functions, and bioinspired applications. Prog. Mater. Sci 88, 467–498 (2017).
72. Libby E et al. Light reflection by the cuticle of C. aurigans scarabs: a biological broadband reflector of left handed circularly polarized light. J. Opt 16, 082001 (2014).
73. Sharma V, Crne M, Park JO & Srinivasarao M Structural origin of circularly polarized iridescence in Jeweled beetles. Science 325, 449–451 (2009). [PubMed: 19628862]
74. Wilts BD, Whitney HM, Glover BJ, Steiner U & Vignolini S Natural helicoidal structures: morphology, self-assembly and optical properties. Mater. Today Proc 1S, 177–185 (2014).
75. Vignolini S et al. Pointillist structural color in Pollia fruit. Proc. Natl Acad. Sci. USA 109, 15712–15715 (2012). [PubMed: 23019355] This paper demonstrates the origin of structural colour in *P. condensata*.
76. Palffy-Muhoray P Liquid crystals New designs in cholesteric colour. Nature 391, 745–746 (1998).

77. Tamaoki N, Parfenov AV, Masaki A & Matsuda H Rewritable full-color recording on a thin solid film of a cholesteric low-molecular-weight compound. Adv. Mater 9, 1102–1104 (1997).
78. de Vries H Rotatory power and other optical properties of certain liquid crystals. Acta Cryst. 4, 219–226 (1951).
79. Habibi Y Key advances in the chemical modification of nanocelluloses. Chem. Soc. Rev 43, 1519–1542 (2014). [PubMed: 24316693]
80. Bordel D, Putaux JL & Heux L Orientation of native cellulose in an electric field. Langmuir 22, 4899–4901 (2006). [PubMed: 16700569]
81. Kimura F et al. Magnetic alignment of the chiral nematic phase of a cellulose microfibril suspension. Langmuir 21, 2034–2037 (2005). [PubMed: 15723507]
82. Blell R et al. Generating inplane orientational order in multilayer films prepared by spray-assisted layer by layer assembly. ACS Nano 11, 84–94 (2017). [PubMed: 28114762]
83. Angelini LG, Lazzeri A, Levita G, Fontanelli D & Bozzi C Ramie (*Boehmeria nivea* (L.) Gaud.) and Spanish Broom (*Spartium junceum* L.) fibres for composite materials: agronomical aspects, morphology and mechanical properties. Ind. Crops Prod 11, 145–161 (2000).
84. Vollrath F & Knight DP Liquid crystalline spinning of spider silk. Nature 410, 541–548 (2001). [PubMed: 11279484]
85. Jin HJ & Kaplan DL Mechanism of silk processing in insects and spiders. Nature 424, 1057–1061 (2003). [PubMed: 12944968]
86. Siró I & Plackett D Microfibrillated cellulose and new nanocomposite materials: a review. Cellulose 17, 459–494 (2010).
87. Tseng P et al. Directed assembly of bio-inspired hierarchical materials with controlled nanofibrillar architectures. Nat. Nanotechnol 12, 474–480 (2017). [PubMed: 28250472] This paper introduces geometric confinement to control nanofibrillar arrangement.
88. Sultan S, Siqueira G, Zimmermann T & Mathew AP 3D printing of nano-cellulosic biomaterials for medical applications. Curr. Opin. Biomed. Eng 2, 29–34 (2017).
89. Suzuki S & Teramoto Y Simple inkjet process to fabricate microstructures of chitinous nanocrystals for cell patterning. Biomacromolecules 18, 1993–1999 (2017). [PubMed: 28505423]
90. Sydney Gladman A, Matsumoto EA, Nuzzo RG, Mahadevan L & Lewis JA Biomimetic 4D printing. Nat. Mater 15, 413–418 (2016). [PubMed: 26808461] This paper describes a programmable 4D printing method to construct nanofibrillar architectures with dynamic response.
91. Håkansson KMO et al. Solidification of 3D printed nanofibril hydrogels into functional 3D cellulose structures. Adv. Mater. Tech 1, 1600096 (2016).
92. Siqueira G et al. Cellulose nanocrystal inks for 3D printing of textured cellular architectures. Adv. Funct. Mater 27, 1604619 (2017).
93. Kokkinis D, Schaffner M & Studart AR Multimaterial magnetically assisted 3D printing of composite materials. Nat. Commun 6, 8643 (2015). [PubMed: 26494528]
94. Li Y et al. 3Dprinted, allinone evaporator for high-efficiency solar steam generation under 1 sun illumination. Adv. Mater 29, 1700981 (2017).
95. Martínez Ávila H, Schwarz S, Rotter N & Gatenholm P 3D bioprinting of human chondrocyte-laden nanocellulose hydrogels for patient-specific auricular cartilage regeneration. Bioprinting 1, 22–35 (2016).
96. Dumais J & Forterre Y “Vegetable dynamicks”: the role of water in plant movements. Annu. Rev. Fluid Mech 44, 453–478 (2012).
97. Forterre Y & Dumais J Generating helices in nature. Science 333, 1715–1716 (2011). [PubMed: 21940886]
98. Elbaum R, Zaltzman L, Burgert I & Fratzl P The role of wheat awns in the seed dispersal unit. Science 316, 884–886 (2007). [PubMed: 17495170]
99. Erb RM, Sander JS, Grisch R & Studart AR Self-shaping composites with programmable bioinspired microstructures. Nat. Commun 4, 1712 (2013). [PubMed: 23591879]
100. Dunlop JW, Weinkamer R & Fratzl P Artful interfaces within biological materials. Mater. Today 14, 70–78 (2011).

101. Burgert I & Fratzl P Actuation systems in plants as prototypes for bioinspired devices. Phil. Trans. A Math. Phys. Eng. Sci 367, 1541–1557 (2009).
102. Studart AR Biologically inspired dynamic material systems. Angew. Chem. Int. Ed 54, 3400–3416 (2015).
103. Armon S, Efrati E, Kupferman R & Sharon E Geometry and mechanics in the opening of chiral seed pods. Science 333, 1726–1730 (2011). [PubMed: 21940888]
104. Majoinen J, Kontturi E, Ikkala O & Gray DG SEM imaging of chiral nematic films cast from cellulose nanocrystal suspensions. Cellulose 19, 1599–1605 (2012).
105. Belamie E, Davidson P & Giraud-Guille MM Structure and chirality of the nematic phase in αchitin suspensions. J. Phys. Chem. B 108, 14991–15000 (2004).
106. Robinson C Liquid-crystalline structures in solutions of a polypeptide. Trans. Faraday Soc 52, 571–592 (1956).
107. Meseck GR, Terpstra AS & MacLachlan MJ Liquid crystal templating of nanomaterials with nature's toolbox. Curr. Opin. Colloid Interface Sci 29, 9–20 (2017).
108. Lagerwall JPF et al. Cellulose nanocrystal-based materials: from liquid crystal self-assembly and glass formation to multifunctional thin films. NPG Asia Mater. 6, e80 (2014).
109. Nguyen TD & MacLachlan MJ Biomimetic chiral nematic mesoporous materials from crab cuticles. Adv. Opt. Mater 2, 1031–1037 (2014).
110. Fernandes SN et al. Mind the microgap in iridescent cellulose nanocrystal films. Adv. Mater 29, 1603560 (2017).
111. Nguyen TD, Peres BU, Carvalho RM & MacLachlan MJ Photonic hydrogels from chiral nematic mesoporous chitosan nanofibril assemblies. Adv. Funct. Mater 26, 2875–2881 (2016).
112. Wu T et al. A bio-inspired cellulose nanocrystal-based nanocomposite photonic film with hyper-reflection and humidity-responsive actuator properties. J. Mater. Chem. C 4, 9687–9696 (2016).
113. Siqueira G, Abdillahi H, Bras J & Dufresne A High reinforcing capability cellulose nanocrystals extracted from Syngonanthus nitens (Capim Dourado). Cellulose 17, 289–298 (2010).
114. Mu X & Gray DG Formation of chiral nematic films from cellulose nanocrystal suspensions is a two-stage process. Langmuir 30, 9256–9260 (2014). [PubMed: 25069681]
115. Shopsowitz KE, Kelly JA, Hamad WY & MacLachlan MJ Biopolymer templated glass with a twist: Controlling the chirality, porosity, and photonic properties of silica with cellulose nanocrystals. Adv. Funct. Mater 24, 327–338 (2014).
116. Nguyen TD, Hamad WY & MacLachlan MJ CdS quantum dots encapsulated in chiral nematic mesoporous silica: New iridescent and luminescent materials. Adv. Funct. Mater 24, 777–783 (2014).
117. Frka-Petesic B, Radavidson H, Jean B & Heux L Dynamically controlled iridescence of cholesteric cellulose nanocrystal suspensions using electric fields. Adv. Mater 29, 1606208 (2017).
118. De France KJ, Yager KG, Hoare T & Cranston ED Cooperative ordering and kinetics of cellulose nanocrystal alignment in a magnetic field. Langmuir 32, 7564–7571 (2016). [PubMed: 27407001]
119. Khan MK et al. Flexible mesoporous photonic resins with tunable chiral nematic structures. Angew. Chem. Int. Ed 52, 8921–8924 (2013).
120. Giese M, Blusch LK, Khan MK, Hamad WY & MacLachlan MJ Responsive mesoporous photonic cellulose films by supramolecular cotemplating. Angew. Chem. Int. Ed 53, 8880–8884 (2014).
121. Yao K, Meng Q, Bulone V & Zhou Q Flexible and responsive chiral nematic cellulose nanocrystal/ poly(ethylene glycol) composite films with uniform and tunable structural color. Adv. Mater 29, 1701323 (2017).
122. Khan MK, Bsoul A, Walus K, Hamad WY & MacLachlan MJ Photonic patterns printed in chiral nematic mesoporous resins. Angew. Chem. Int. Ed 54, 4304–4308 (2015).
123. Khan MK, Hamad WY & MacLachlan MJ Tunable mesoporous bilayer photonic resins with chiral nematic structures and actuator properties. Adv. Mater 26, 2323–2328 (2014). [PubMed: 24446312]

124. Kelly JA, Yu M, Hamad WY & MacLachlan, Large MJ crack-free freestanding films with chiral nematic structures. Adv. Opt. Mater 1, 295–299 (2013).
125. Shopsowitz KE, Qi H, Hamad WY & MacLachlan MJ Free-standing mesoporous silica films with tunable chiral nematic structures. Nature 468, 422–425 (2010). [PubMed: 21085176] The paper discusses chiral nematic cellulose nanocrystals as templates for mesoporous structures.
126. Shopsowitz KE, Hamad WY & MacLachlan MJ Flexible and iridescent chiral nematic mesoporous organosilica films. J. Am. Chem. Soc 134, 867–870 (2012). [PubMed: 22188398]
127. Shopsowitz KE, Hamad WY & MacLachlan MJ Chiral nematic mesoporous carbon derived from nanocrystalline cellulose. Angew. Chem. Int. Ed 50, 10991–10995 (2011).
128. Shopsowitz KE, Stahl A, Hamad WY & MacLachlan MJ Hard templating of nanocrystalline titanium dioxide with chiral nematic ordering. Angew. Chem. Int. Ed 51, 6886–6890 (2012).
129. Schlesinger M, Giese M, Blusch LK, Hamad WY & MacLachlan MJ Chiral nematic cellulose-gold nanoparticle composites from mesoporous photonic cellulose. Chem. Commun 51, 530–533 (2015).
130. Qi H, Shopsowitz KE, Hamad WY & MacLachlan MJ Chiral nematic assemblies of silver nanoparticles in mesoporous silica thin films. J. Am. Chem. Soc 133, 3728–3731 (2011). [PubMed: 21355559]
131. Kelly JA et al. Responsive photonic hydrogels based on nanocrystalline cellulose. Angew. Chem. Int. Ed 52, 8912–8916 (2013).
132. Parker RM et al. Hierarchical self-assembly of cellulose nanocrystals in a confined geometry. ACS Nano 10, 8443–8449 (2016). [PubMed: 27564644] This paper introduces the geometrically confined self-assembly of cellulose nanocrystals.
133. Li Y et al. Colloidal cholesteric liquid crystal in spherical confinement. Nat. Commun 7, 12520 (2016). [PubMed: 27561545]
134. Jativa F, Schutz C, Bergstrom L, Zhang X & Wicklein B Confined self-assembly of cellulose nanocrystals in a shrinking droplet. Soft Matter 11, 5374–5380 (2015). [PubMed: 26059700]
135. Wang PX, Hamad WY & MacLachlan MJ Polymer and mesoporous silica microspheres with chiral nematic order from cellulose nanocrystals. Angew. Chem. Int. Ed 55, 12460–12464 (2016).
136. Cranford SW & Buehler MJ Biomateriomics. Springer Series in Materials Science, Vol. 165 (Springer Science & Business Media, Heidelberg, 2012).
137. Buehler MJ & Yung YC Deformation and failure of protein materials in physiologically extreme conditions and disease. Nat. Mater 8, 175–188 (2009). [PubMed: 19229265]
138. Huang PS, Boyken SE & Baker D The coming of age of de novo protein design. Nature 537, 320–327 (2016). [PubMed: 27629638]
139. Kaltofen S et al. Computational de novo design of a self-assembling peptide with predefined structure. J. Mol. Biol 427, 550–562 (2015). [PubMed: 25498388]
140. López de la Paz M et al. De novo designed peptide-based amyloid fibrils. Proc. Natl Acad. Sci. USA 99, 16052–16057 (2002). [PubMed: 12456886]
141. Zhang HV et al. Computationally designed peptides for self-assembly of nanostructured lattices. Sci. Adv 2, 1600307 (2016).
142. Gallardo R et al. De novo design of a biologically active amyloid. Science 354, aah4949 (2016). [PubMed: 27846578]
143. Huang W et al. Synergistic integration of experimental and simulation approaches for the de novo design of silk-based materials. Acc. Chem. Res 50, 866–876 (2017). [PubMed: 28191922]
144. Lin S et al. Predictive modelling-based design and experiments for synthesis and spinning of bioinspired silk fibres. Nat. Commun 6, 6892 (2015). [PubMed: 26017575]
145. Tarakanova A, Huang W, Weiss AS, Kaplan DL & Buehler MJ Computational smart polymer design based on elastin protein mutability. Biomaterials 127, 49–60 (2017). [PubMed: 28279921]
146. Huang W et al. Design of multistimuli responsive hydrogels using integrated modeling and genetically engineered silk–elastin-like proteins. Adv. Funct. Mater 26, 4113–4123 (2016). [PubMed: 28670244]

147. Ling S, Li C, Jin K, Kaplan DL & Buehler MJ Liquid exfoliated natural silk nanofibrils: applications in optical and electrical devices. Adv. Mater 28, 7783–7790 (2016). [PubMed: 27352291]

148. Ling S et al. Modulating materials by orthogonally oriented βstrands: Composites of amyloid and silk fibroin fibrils. Adv. Mater 26, 4569–4574 (2014). [PubMed: 24845975]

149. Ling S, Jin K, Kaplan DL & Buehler MJ Ultrathin free-standing *Bombyx mori* silk nanofibril membranes. Nano Lett 16, 3795–3800 (2016). [PubMed: 27076389]

150. Toivonen MS, Kaskela A, Rojas OJ, Kauppinen EI & Ikkala O Ambient-dried cellulose nanofibril aerogel membranes with high tensile strength and their use for aerosol collection and templates for transparent, flexible devices. Adv. Funct. Mater 25, 6618–6626 (2015).

151. Mounet N et al. Two-dimensional materials from high-throughput computational exfoliation of experimentally known compounds. Nat. Nanotechnol 10.1038/s41565-017-0035-5 (2018).

152. Arvidsson R, Nguyen D & Svanström M Life cycle assessment of cellulose nanofibrils production by mechanical treatment and two different pretreatment processes. Environ. Sci. Technol 49, 6881–6890 (2015). [PubMed: 25938258]

153. Li Q, McGinnis S, Sydnor C, Wong A & Renneckar S Nanocellulose life cycle assessment. ACS Sustain. *Chem. Eng.* 1, 919–928 (2013).

154. Zhu Y, Romain C & Williams CK Sustainable polymers from renewable resources. Nature 540, 354–362 (2016). [PubMed: 27974763]

155. Ehrlich H Chitin and collagen as universal and alternative templates in biomineralization. Int. Geol. Rev 52, 661–699 (2010).

156. Barthelat F, Yin Z & Buehler MJ Structure and mechanics of interfaces in biological materials. Nat. Rev. Mater 1, 16007 (2016).

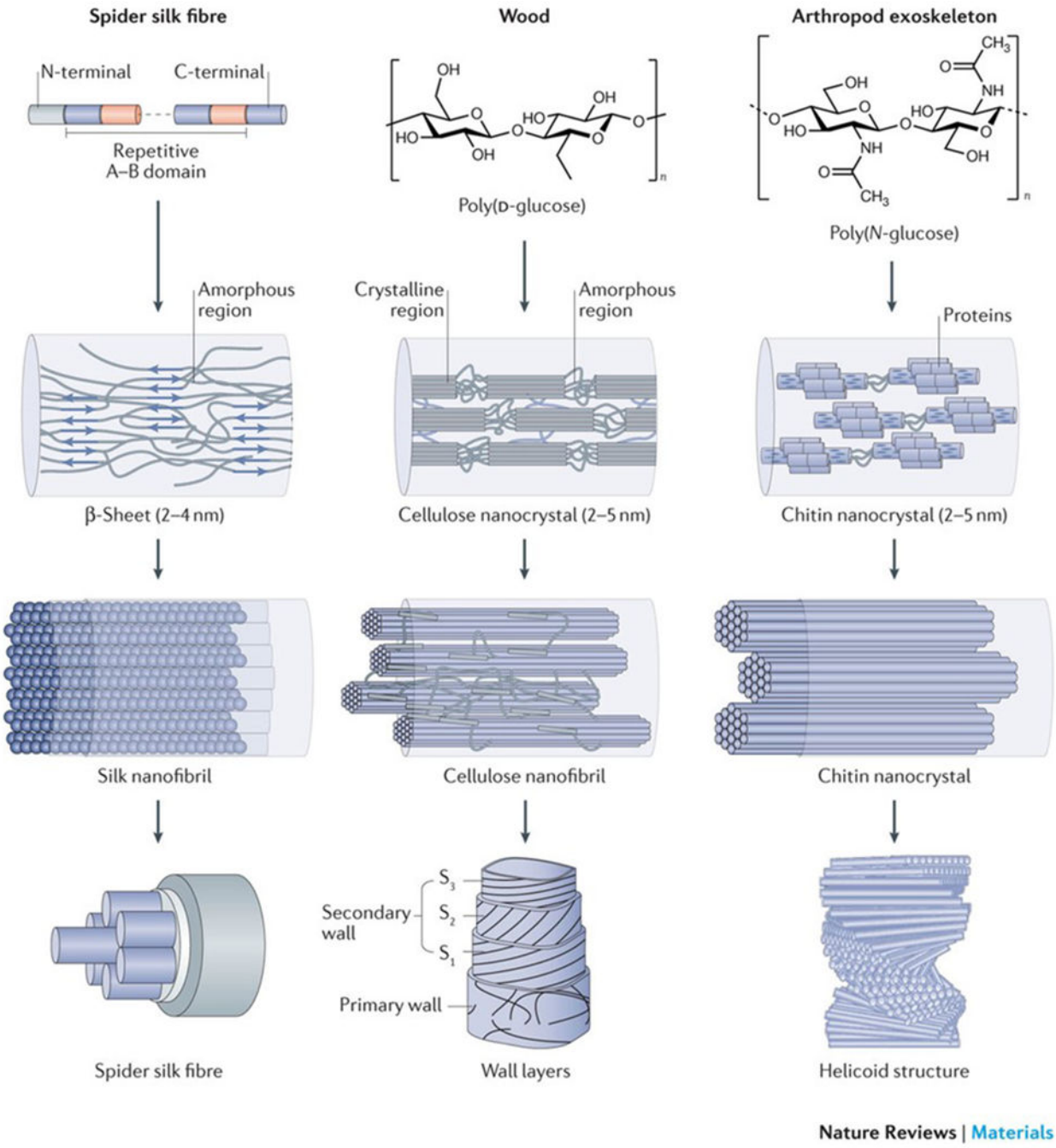

Figure 1|. Hierarchical structure of silk, cellulose and chitin.

Silk, wood and exoskeletons of arthropods are formed following the same multiscale construction principle. The smallest units of silk fibrils are highly repetitive core sequences of amino acids with hydrophilic and hydrophobic segments (repetitive A–B domain), which are flanked by terminal domains (N-terminal and C-terminal)[14]. The hydrophilic domains assemble into random coils and/or helical structures, and the hydrophobic domains transition into β-sheet structures. Cellulose consists of a linear chain of β-(1,4)-linked d-glucose units[4,5], and chitin is made of a long-chain polymer of (1,4)-β-*N*-acetylglucosamine[155]. The

nanocrystal size of the respective crystalline units is confined to several nanometres. The nanocrystals assemble into fibrils with an orientation along the longitudinal axis, which can be further organized into 2D laminar and 3D helicoidal architectures at the micrometre scale in silk fibres, cell wall layers and exoskeletons. S, secondary wall layer. The wall layers are reproduced from REF. 156, Macmillan Publishers Limited. The helicoid structure is adapted with permission from REF. 63, Elsevier.

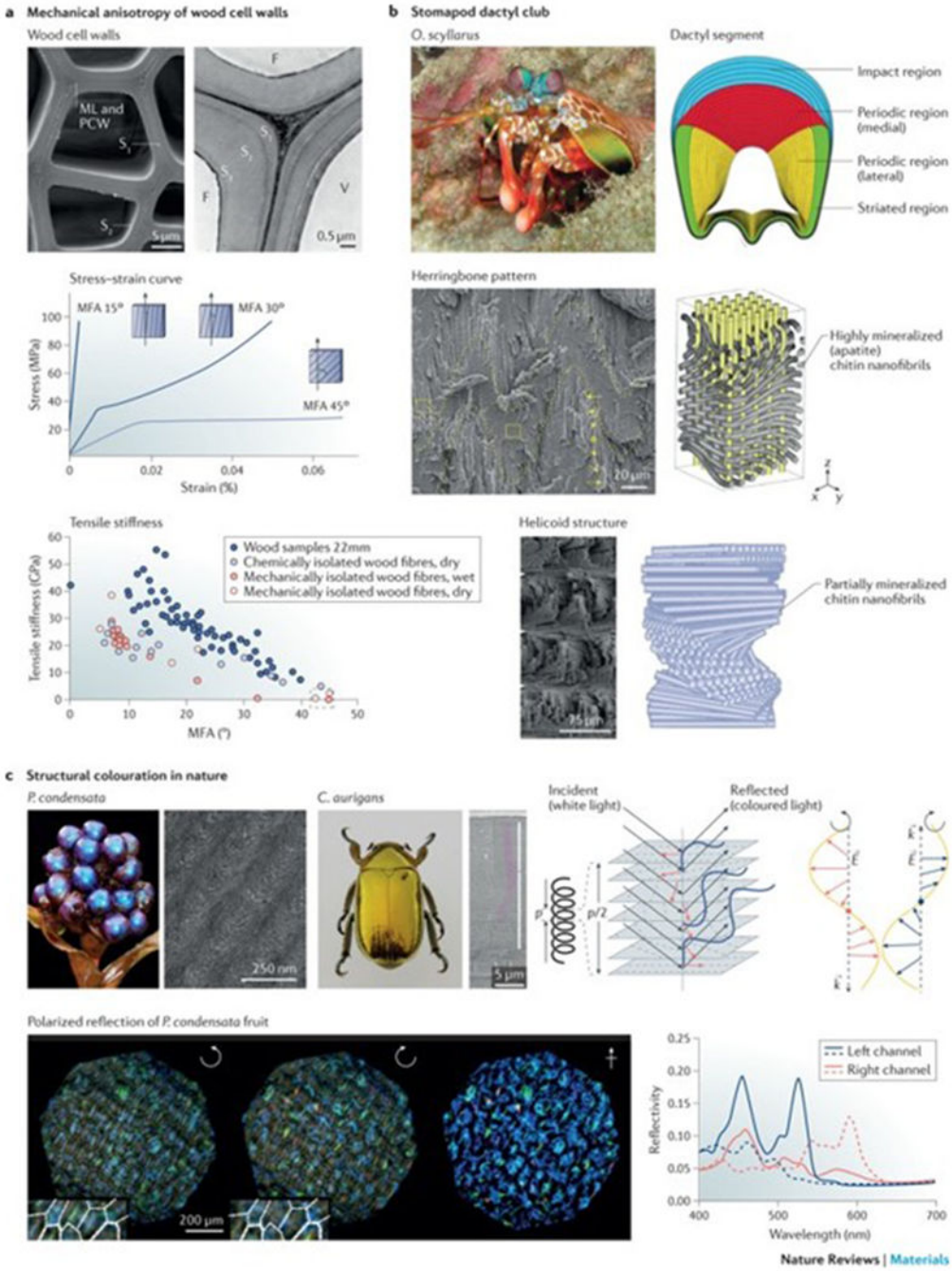

Figure 2|. Nanoconfinement and mechanical properties of silk.

a | Stress–strain curves of a dragline silk fibre produced by the spider *Nephila edulis* (*N. edulis*), of a silk fibre produced by the silkworm *Bombyx mori* (*B. mori*) and of the para-aramid synthetic fibre Kevlar 46. **b** | Force–displacement and stress–strain curves of β-sheet nanocrystals of silk fibres with different dimensions. **c** | Fracture mechanisms of differently aligned β-sheet nanocrystals calculated by pull-out simulations. Snapshots were taken just before and after rupture of the hydrogen bonds. The left snapshot shows the failure of a large β-sheet nanocrystal (consisting of 15 strands with L = 6.56 nm, in which L is the size of the

nanocrystal in the *y* direction); the right snapshot shows the failure of a small β-sheet nanocrystal (consisting of seven strands with $L = 2.83$ nm). The long structures (left) fail by considerable bending, and the short structures (right) by a stick–slip motion (indicated by arrows). **d** | The dimensions of β-sheet nanocrystals affect the mechanical properties of silk fibres. The schematic phase diagram shows the formation of confined nanocrystals with critical strand length (h^*) and critical nanocrystal size (L^*), leading to the maximal strength stiffness and toughness of the material. **e** | The correlation between the length (h) of a β-strand and L illustrates how nanoconfinement affects hydrogen bonding and the mechanical properties. F, strength of nanocrystal; S, strength of the β-strand; T, toughness of the nanocrystal. Part **a** is adapted with permission from REF. 11, RSC. Part **b** is reproduced with permission from REF. 45, American Chemical Society. Parts **c**, **d** and **e** are reproduced from REF. 8, Macmillan Publishers Limited.

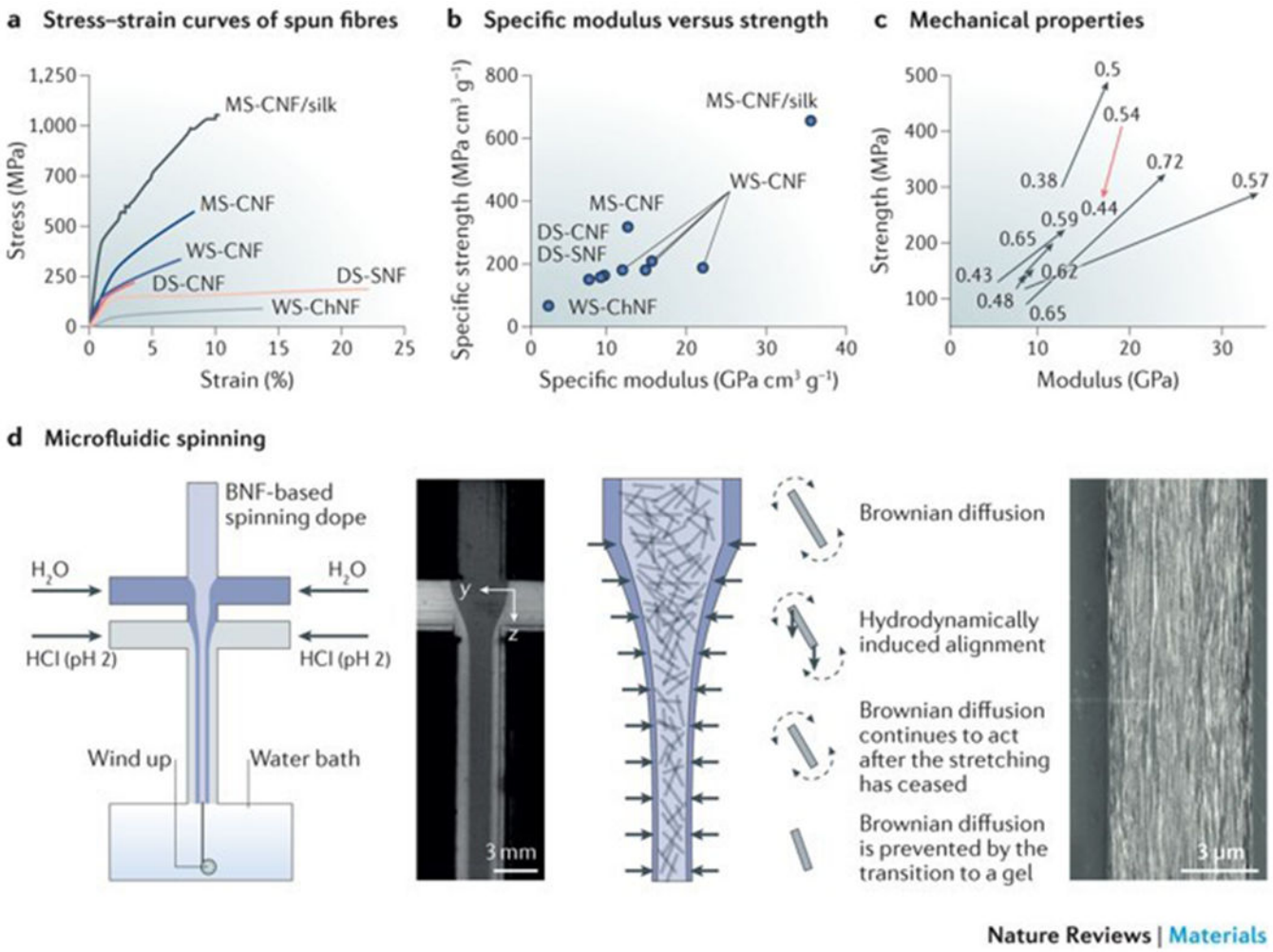

Figure 3|. Mechanical and optical properties of nanofibrils.

a | The scanning electron microscopy (SEM) image shows the cross-sectional morphology of a wood cell wall, which is composed of three layers (S_1, S_2 and S_3). The stress–strain curves illustrate the correlation between the microfibril angle (MFA) and the stress–strain behaviour of different wood tissues. The relationship between the MFA and the tensile stiffness is shown for single wood fibres isolated by different methods. The same trend of decreasing tensile moduli with increasing MFA of the wood fibres is seen under both wet and dry conditions, despite these fibres being isolated by different techniques. **b** | Structural features of the dactyl club of the peacock mantis shrimp *Odontodactylus scyllarus* (*O. scyllarus*). The cross section of the club shows the impact region (blue), the medial periodic region (red), the lateral periodic region (yellow) and the striated region (green). The impact region is formed by mineralized chitin nanofibrils arranged in a herringbone pattern. The periodic region is formed by partially mineralized chitin nanofibrils assembled in a helicoidal structure, as illustrated in the schematics and SEM images. **c** | Photographs and SEM images of *Pollia condensata* (*P. condensata*) and the scarab *Chrysina aurigans* (*C. aurigans*) illustrate structural colour enabled through the helicoidal arrangement of biopolymer nanofibrils. A left-handed helicoid reflects left-handed circularly polarized light

(blue), in which the wavevector *k* depends on the pitch *p*, which is the distance between two planes with the same fibril orientation. The dashed lines indicate the typical arch pattern observed in anatomical cross sections. Right-hand circularly polarized light (red) is transmitted through the left-handed helicoidal structure. *E*, electric field vector; F, fibre; ML, middle lamella; PCW, primary cell wall; V, vessel. Part **a** is reproduced with permission from REF 49, Elsevier; adapted with permission from REF. 50, Elsevier; and reproduced from REFS 52,53, Macmillan Publishers Limited. Part **b** is reproduced with permission from REFS 65,68, AAAS and John Wiley and Sons, respectively. Part **c** is reproduced with permission from REFS 72,75, IOP Publishing and Proceedings of the National Academy of Sciences, respectively; and adpated from REF. 76, Macmillan Publishers Limited.

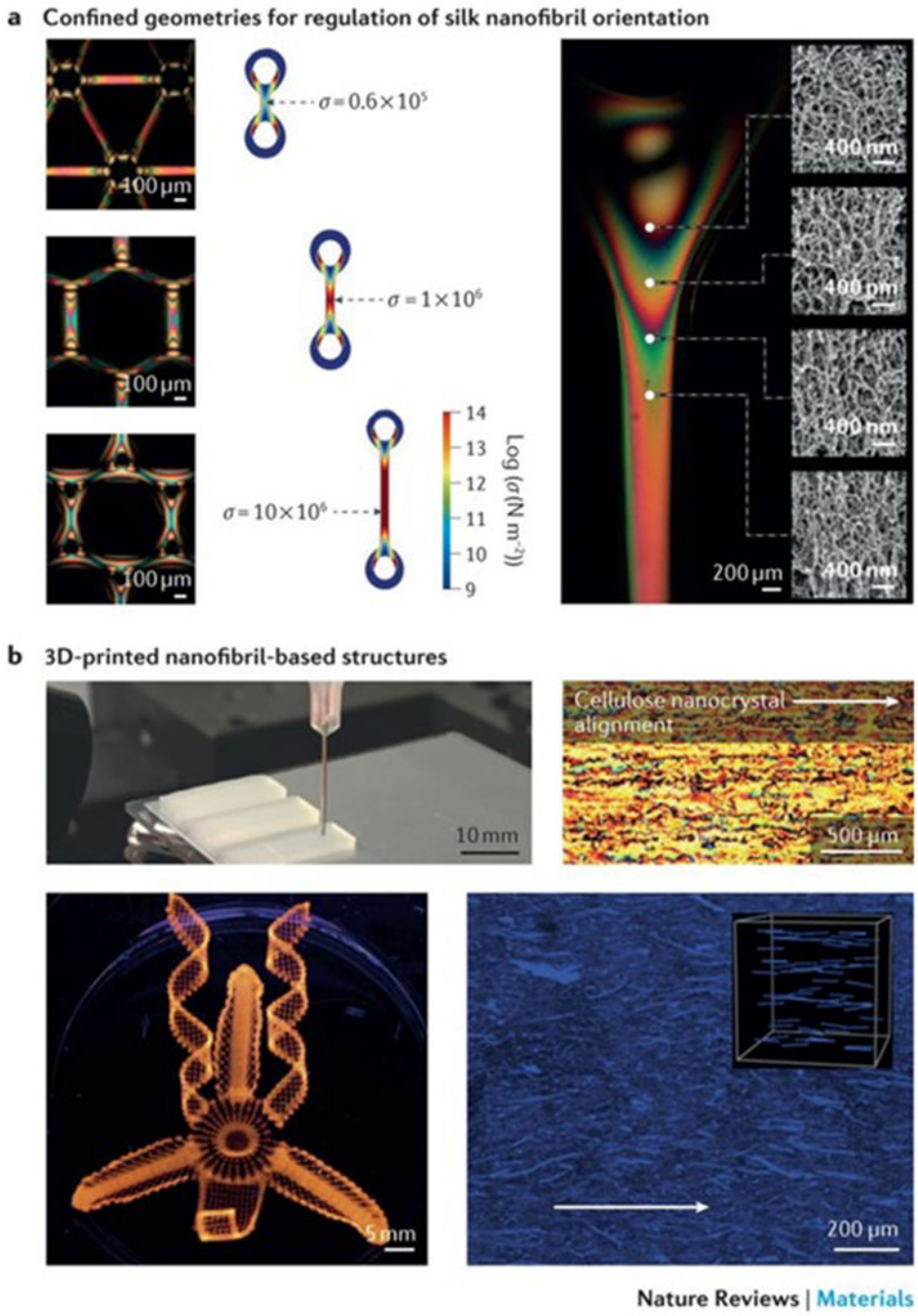

Figure 4|. Artificial spinning of biopolymer nanofibrils.

a | The stress–strain curves of biopolymer nanofibril fibres illustrate the differences in the stress–strain behaviour of fibres produced by wet spinning (WS), dry spinning (DS) or microfluidic spinning (MS). **b** | These differences are also reflected in the relationship between the specific elastic modulus and the specific strength of the fibres. **c** | The orientation index (or order parameter) of the fibrillar structures has an effect on the strength and elastic modulus of the fibres. **d** | Microfluidic spinning can be applied to regulate the orientation of biopolymer nanofibrils. The nanofibrils in the focused flow are illustrated as

rods (the fibril length in relation to the channel width is exaggerated by a factor of approximately 300). The diffusion of Na^+ (blue) is added in the form of NaCl in the focusing liquid. In a microfluidic spinning device, the nanofibrils in the spinning dope are free to rotate owing to strong electrostatic repulsion, and they align towards the accelerating flow direction. The hydrodynamical, molecular and electrochemical processes involve Brownian diffusion (dashed arrows) and hydrodynamically induced alignment (solid arrows). The scanning electron microscopy image shows the surface of a cellulose nanofibril-based regenerated fibre. BNF, biopolymer nanofibril; ChNF, chitin nanofibril; CNF, cellulose nanofibril; SNF, silk nanofibril. The stress–strain curves in part **a** are drawn using the stress–strain curves data from REFS 27,30,33–36. Parts **b** and **c** use data from REFS 27,30,33–36. Panel **d** is reproduced and adapted from REFS 35, CC-BY-3.0; and adpated from REF. 36, CC-BY-4.0.

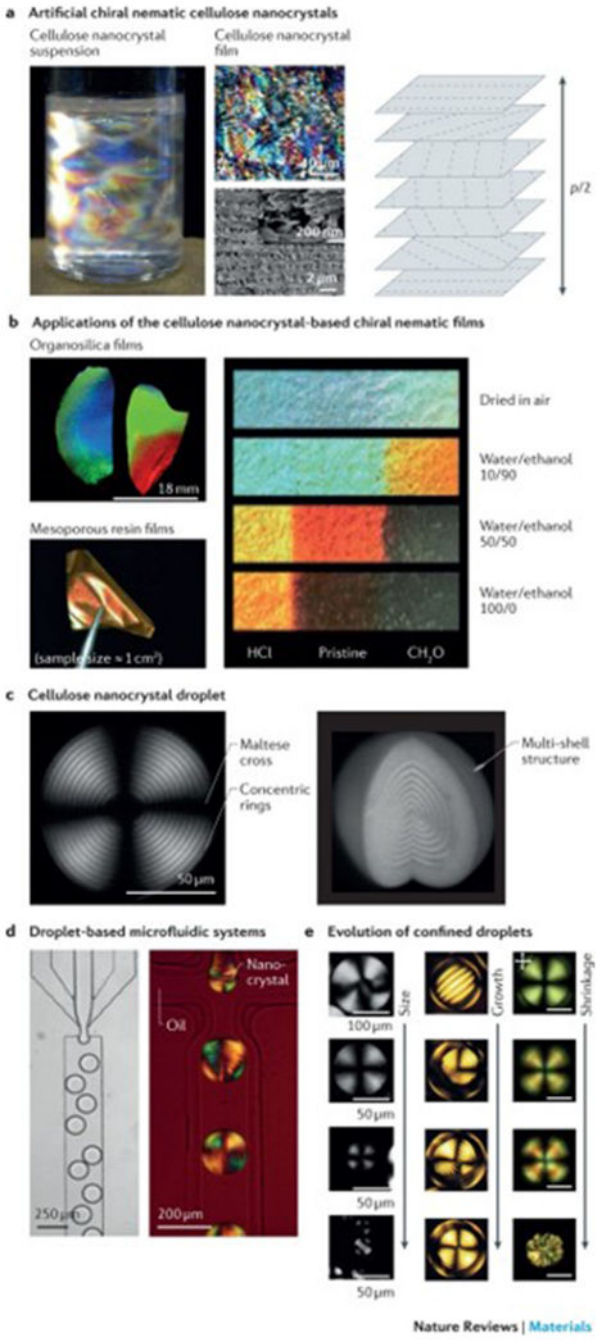

Figure 5|. 2D and 3D nanofibril fabrication.

a | Optically anisotropic silk nanofibrils can be generated by fabricating specific periodic shapes, for example, through confinement by polydimethylsiloxane-moulded rings. In these rings, mechanical tension can be introduced by either contraction in ethanol and water or through direct deformation. Finite element simulations illustrate the stress (σ) distribution in fibres, anchored through the rings, which are spaced by 250, 1,125 and 3,125 μm, respectively. The fibres undergo a 33% contraction in size. The scanning electron microscopy images show the birefringence and corresponding internal nanofibrillar

morphology of a ring-anchored fibre. Mechanical stress causes an increase in birefringence and a change in the orientation of the silk nanofibrils. **b** | 3D printing techniques can be applied to regulate the site-specific 3D alignment of biopolymer nanofibrils. The photograph shows a 3D-printed block composed of parallel lines of cellulose in eight layers; the cross-polarized optical microscopy image shows the top view of the block. Complex orchid-inspired flower morphologies can be generated by 3D printing. The dynamics of the printed flower result from the cellulose nanofibril orientation, as illustrated in the micrograph. Part **a** is reproduced from REF. 87, Macmillan Publishers Limited. Part **b** is reproduced with permission from REF. 90,92, Macmillan Publishers Limited and John Wiley and Sons, respectively.

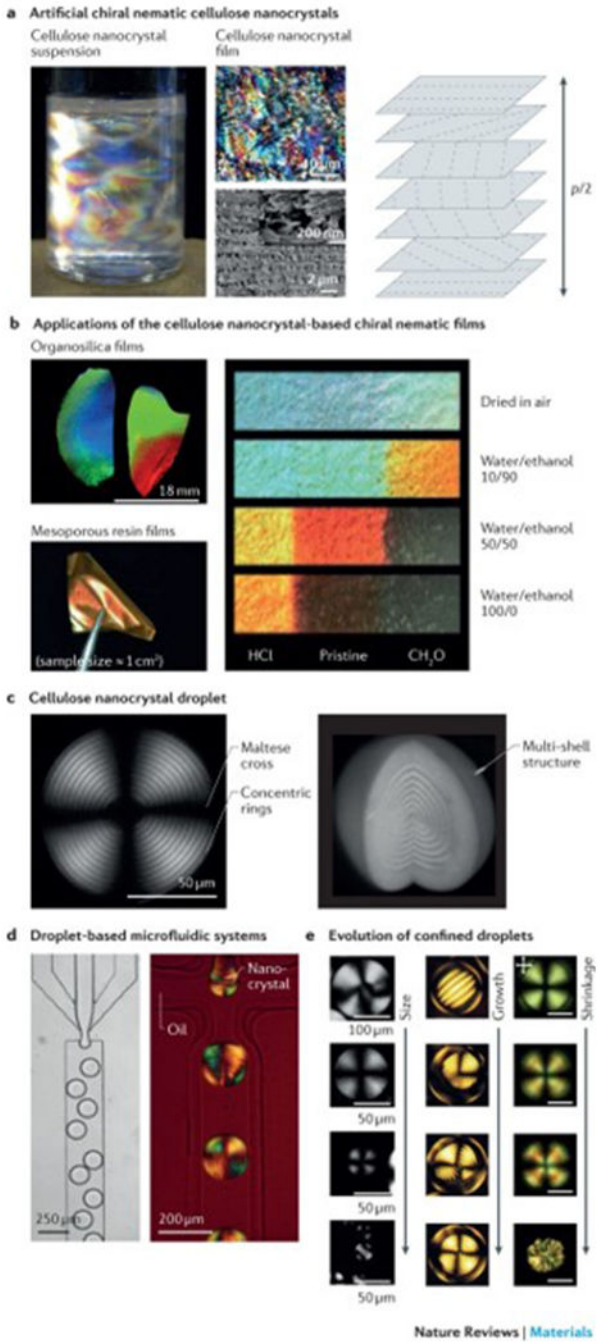

Figure 6|. Structural colour of anisotropic nanofibrils.

a | Artificial chiral nematic cellulose nanocrystal suspensions and films feature structural colour when *p*/2 corresponds to a wavelength of visible light (400–700 nm), in which the pitch, *p,* is the distance between two planes with the same fibril orientation. The photograph shows an aqueous dispersion of cellulose nanocrystals (0.50 (w/v)) with birefringent domains caused by cross-polarized light. The optical microscopy and scanning electron microscopy (SEM) images illustrate the fractured surface across the film. The high-resolution SEM image of the fractured surface is shown in the inset. **b** | The photographs

show organosilica and mesoporous resin films of chiral nematic cellulose nanocrystal templates. Strips (centimetre scale) of mesoporous resin films show the different colours achieved by treatment with binary water/ethanol mixtures. The left and right ends of the strips were treated with HCl and CH_2O, respectively, and the middle region remained untreated. **c** | Polarizing optical microscopy (POM) images of a chiral nematic cellulose nanocrystal droplet with a diameter of 154 μm and a height of 118 μm show the multilayer structure and the typical pattern of concentric rings and crosses. **d** | Droplet-based microfluidic systems can be applied to generate droplets in the chiral nematic cellulose nanocrystal phase, as illustrated in the optical microscopy image. The POM image shows the microfluidic generation of water-in-oil droplets using a 14.5% (w/v) suspension of cellulose nanocrystals. **e** | Representative POM images of chiral nematic cellulose nanocrystals show the structural evolution of nanocrystal droplets or tactoid microgels. Left panel: cellulose nanocrystal droplets with sizes ranging from radius R = 130 μm (first image), 40≤R≤ 115 μm (second image), 10 ≤R≤ 40 μm (third image) to R ≤10 μm (fourth image). Middle panel: microgels of cellulose nanocrystal tactoids with diameters of 69 μm, 136 μm, 142 μm and 141 μm. Right panel: shrinkage evolution of confined chiral nematic cellulose nanocrystal droplets. Scale bars = 50 μm. Part **a** is reproduced from REFS 104,113, Macmillan Publishers Limited. Part **b** is reproduced with permission from REF. 126, American Chemical Society; and reproduced with permission from REFS 119,122, John Wiley and Sons. Part **c** is reproduced from REF. 133, CC-BY-4.0; and reproduced with permission from REF. 135, John Wiley and Sons. Part **d** is reproduced from REFS 132,133, CC-BY-4.0. Part **e** is reproduced from REFS 132,133, CC-BY-4.0; and reproduced with permission from REF. 135, John Wiley and Sons.

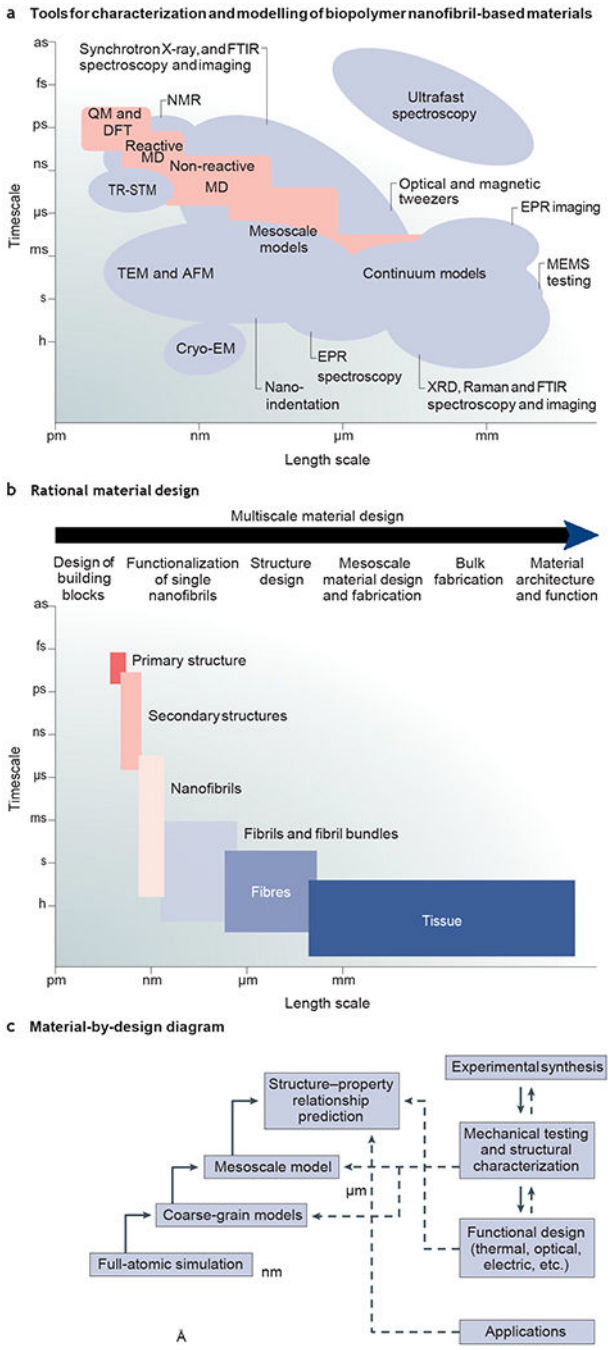

Figure 7|. Rational design of nanofibrillar materials.

a | Theoretical and experimental approaches for the rational design of nanofibrillar materials. **b** | Multiscale material design strategy. **c** | Material-by-design paradigm. AFM, atomic force microscopy; CryoEM, cryoelectron microscopy; DFT, density functional theory; EPR, electron paramagnetic resonance; FTIR, Fourier transform infrared spectroscopy; MD, material design; MEMS, microelectromechanical systems; QM, quantum mechanics; TEM,

transmission electron microscopy; TRSTM, thermal radiation scanning tunnelling microscopy; XRD, X-ray diffraction.